BEHAVIOUR OF PLASTERED STRAW-BALE ASSEMBLIES SUBJECTED TO THREE-POINT BENDING

Michael Rakowski, M.Sc.[1] and Colin MacDougall, PhD, P.Eng.[2]

ABSTRACT

The search for more sustainable construction methods has renewed interest in straw-bale construction. Rectangular straw bales stacked in a running bond and plastered on the interior and exterior faces have been shown to have adequate strength to resist typical loads found in one- and two-storey structures. The straw bales provide excellent insulation, while possessing low embodied energy compared to conventional insulation materials.

The structural behaviour of a load-bearing plastered straw-bale wall subject to uniform compressive loading has been the focus of a number of studies reported in the literature. However, in a typical building wall, there will be numerous locations (such as around window and door openings) where the load paths produce areas of concentrated stress. The behaviour in these regions cannot necessarily be predicted using tests from uniformly loaded wall assemblies.

This paper describes experiments on plastered single bale assemblies subjected to three-point bending. These assemblies develop shear and flexural stresses, and so simulate the stresses that exist around door and window openings in a wall. The specimens were rendered with lime-cement plaster, and were either unreinforced, or contained steel "diamond lath" mesh embedded within the plaster. The specimens were pin-supported at various centre-to-centre distances (L) ranging from 200 mm to 500 mm. The height (H) of all specimens was constant at 330 mm. This gave a range of H/L values of 0.66 to 1.65.

Two distinct types of failure were observed. For tests with H/L < 1, failure was due to flexural tension cracks in the plaster which propagated through the depth of the plaster skin. For tests with H/L > 1, failure was due to crushing of the plaster in compression under one of the loading points.

It was shown that models based on simple mechanics were able to adequately predict the assembly strength. In particular, analysing the assemblies with H/L < 1 as simple beams, and using the transformed section concept to deal with the straw and steel mesh, was adequate for predicting their strength.

[1]Junior Engineer, Kiewit-Alarie, Kapuskasing, Ontario, Canada, mr.rakowski@kiewit.com
[2]Associate Professor, Department of Civil Engineering, Queen's University, Kingston, Ontario, Canada, colin@civil.queensu.ca

The results suggest that current practice for straw bale construction is generally appropriate. To avoid tensile cracking of plaster due to flexure, regions around doors, windows, and other openings should be designed such that H/L > 1. In regions where H/L < 1, the use of steel reinforcing mesh can increase the plastered bale strength by 30% on average.

KEYWORDS
straw bale construction, cement-lime plaster, discontinuous regions, structural testing, 3-point bending

INTRODUCTION

In the green building and sustainable construction community, straw-bale construction is one of a number of so-called "natural building" techniques. Others include, for example, rammed earth, adobe, and hemp-lime. "Straw" in this context refers to the dried tubular stalk of a plant connecting the roots to the grain head of the plant. It is produced as a by-product of grain production and usually baled. A typical load-bearing straw-bale wall (Figure 1) is built by stacking bales of straw (typical dimensions 0.4 m × 0.5 m × 1.0 m, density ranging between 80 kg/m^3 to 120 kg/m^3) in a running bond. A top (or sill) plate, usually constructed of wood, is placed on the bales. Straps running from the top plate to the bottom plate, Figure 2, are typically used to precompress the bale to reduce straw settlement and to level the top plate (King 2006). A wire or plastic mesh may be affixed to the straw and top and bottom plates to improve the ductility of the wall in seismically active regions. Plaster with a nominal thickness between 37 mm and 50 mm is then applied to the straw. Plasters may include cement-lime, lime, or earthen plasters (King 2006). The straw bales provide insulation, while the plaster protects the bales from moisture and provides strength and stiffness for the wall. However, because of the bonding between the straw and plaster, the straw also provides lateral support for the thin plaster skins, ensuring that failure of a wall is dominated by compression failure of the plaster, rather than local buckling of the plaster (King 2006, Vardy and MacDougall 2006).

FIGURE 1. Details of a typical load-bearing straw bale wall.

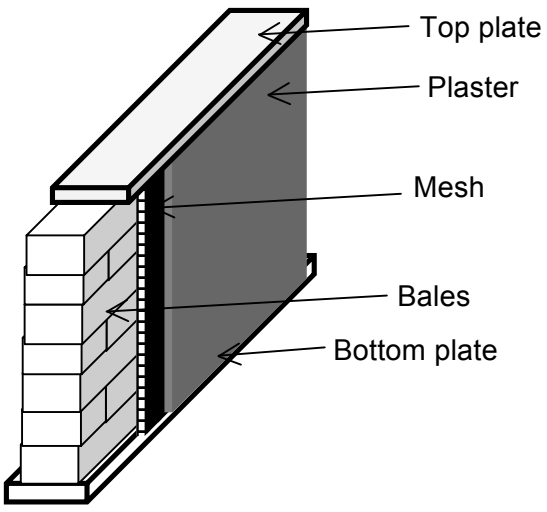

Not all straw-bale construction is load bearing. In some cases, the plastered straw bales may be used to infill a structural frame (which is usually timber). The plastered straw bales are primarily insulation in these applications, although of course they must carry some structural loads, such as self-weight and wind loads.

Straw has been used by humans in construction for thousands of years (e.g. straw mixed with clay to form bricks), however the use of baled straw only dates back about 100

years. The period since the early 1990s has seen a revival in interest in straw-bale construction. Thousands of straw-bale buildings have been constructed, from self-built homes to larger public buildings. Pre-fabricated straw-bale panels have been successfully integrated into conventional timber and concrete frames as well (Figure 3).

There have been numerous ad-hoc tests conducted in the past 2 decades on various straw-bale assemblies to quantify the strength of these walls. Many of these, while providing useful data, have been unpublished. A comprehensive summary of these test results is provided by King (2006). In terms of published data, Ashour et al. (2010) examined the compressive strength of plasters typically used for straw bale construction. Vardy and MacDougall (2007) and Vardy (2009) developed and validated models for predicting the compressive strength of straw-bale assemblies when subjected to concentric and eccentric in-plane loading. Gross et al. (2009) performed racking tests of plastered straw bale walls. Kim et al. (2011) tested single plastered straw bales in compression.

Testing to date has for the most part been on plastered straw-bale assemblies subjected to uniform compressive in-plane loading leading to essentially uniform compressive stress. This is important for establishing the basic strength of straw-bale walls. However, in a typical building, there will be numerous regions in the wall where the in-plane loading and geometry lead to non-uniform stresses. Typical examples are the region above a window (Figure 4) or the region above a door opening. Literature related to reinforced concrete refers to such situations as "discontinuous regions" (MacGregor and Bartlett and 1999, for example). Generally, the behavior in a discontinuous region will depend on the ratio of the depth (H) to the length (L) of the region. For regions with a low H/L, bending and flexural stresses tend to dominate. For regions with a high H/L, arching action and shear stresses tend to dominate. For reinforced concrete, recourse is often made to strut-and-tie models to design discontinuous regions (MacGregor and Bartlett 1999).

There is currently little guidance for structural engineers for the analysis of discontinuous regions in straw-bale walls. The most relevant work has been by Parker et al. (2006)

FIGURE 2. Details of the strapping used for a load-bearing straw bale wall.

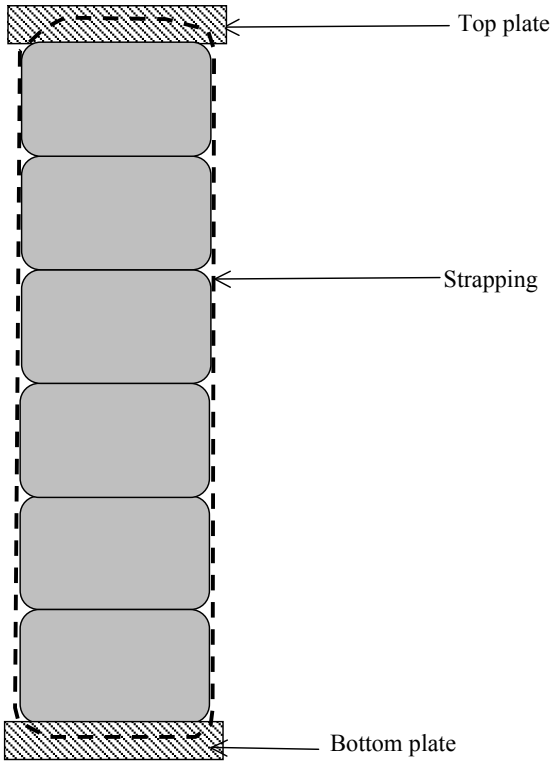

FIGURE 3. Prefabricated straw bale panels used for residential construction.

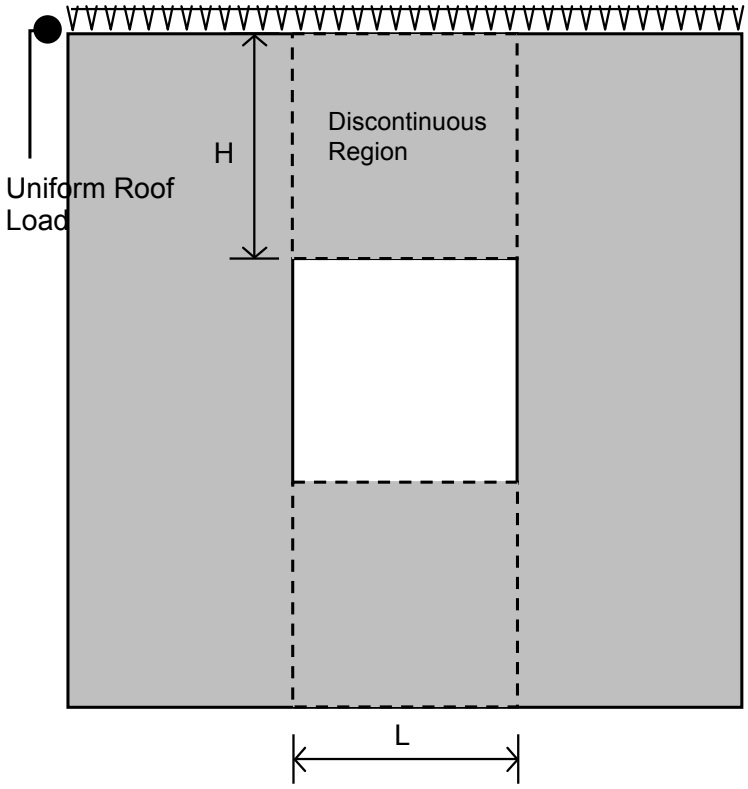

FIGURE 4. A typical "discontinuous" region in a building wall.

which examined details for anchoring reinforcing mesh for straw bale walls. This however, was focused on the mesh and methods to attach it to the top or bottom plates, rather than the performance of the plastered straw bale wall per se. The objective of the work described in this paper is to investigate the mechanics of single plastered straw-bale assemblies in a simulated "discontinuous" region. This is done by subjecting the bales to 3-point bending. The work consists of 12 tests of plastered straw bales. The materials, test set-up, and results are described in the remainder of the paper.

MATERIALS AND TEST PROCEDURE

Two-string rectangular wheat bales were sourced from local farms and stored in a cool, dry area throughout the experimental process. Before fabrication, the bales had bulk densities ranging from 78 to 112 kg/m^3 and measured 375 ± 10 mm high, 475 ± 10 mm wide, and 700 ± 50 mm long.

The plaster used for each of the nine specimens was a lime-cement plaster with volumetric proportions of 6 : 1 : 1 of sand, cement, and lime, respectively. The use of volumetric proportions is typical of straw-bale construction practice and so was adopted here. The water to cementitious materials (w/cm) ratio of the plaster was 1.80, by mass. The sand was completely dry masonry sand, and the water was from the laboratory tap.

The cementitious materials were part of a typical mortar mix, Mason's Choice High Bond Portland Lime Type N, which is a mixture of equal parts by mass of Type I Portland cement (ASTM C150 2007a) and hydrated lime (ASTM C207 2006).

Each plastered straw-bale assembly was assembled in a steel frame to ensure consistent dimensions (Figure 5). The bales were trimmed to a thickness of 400 ± 10 mm and were compressed in the frame to a height of 330 mm. The bales were laid flat (i.e. straw stalks were horizontal). Two plastic strips were installed on each of the two plastering surfaces. The strips were the same height as the bale, were 25 mm thick, and were placed 600 ± 1 mm apart. The plastic strips helped maintain consistent nominal plaster skin dimensions, 600 by 330 by 25 mm, for all specimens.

FIGURE 5. Frame for fabricating straw bale test specimens.

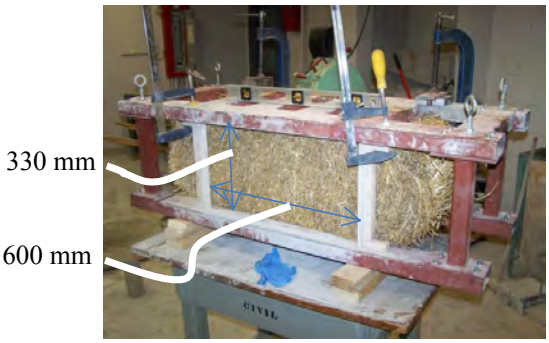

Figure 6 shows the detail of a typical straw-bale wall window opening. Various types of wire mesh are often affixed to the straw before plastering in order to improve bond and bridge any cracks that may occur in the plaster in this region. To investigate the effect of wire mesh, three of the specimens were reinforced with a sheet of galvanized diamond metal lath. The lath used in this study was composed of 2 mm by 1 mm rectangular strands. The height and width of the diamond-shaped openings were 8 mm and 12 mm respectively and the sheet weighed 0.95 kg/m^2. The lath was manufactured by Bailey Metal Products Limited. If a bale was to be reinforced, the diamond metal mesh lath was wrapped tightly around the bale. Following typical straw-bale construction practice, a baling needle was used to thread "baling twine" through the bale and connect the opposing lath surfaces. The baling twine is standard sisal fibre used for baling straw or hay. The twine was then tied tight to achieve tight, flush contact between the lath and the bale (Figure 7) by threading through the bale approximately every 100 mm.

FIGURE 6. Detail of a typical window opening in a straw bale wall.

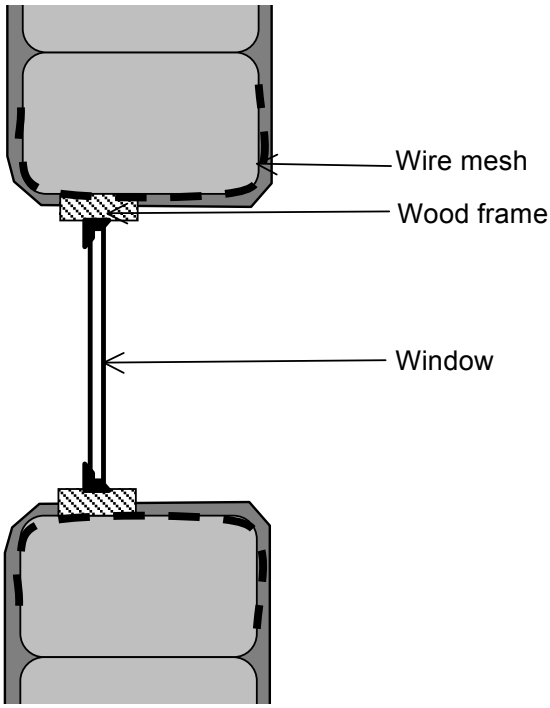

Plaster was applied in three layers. The first layer was worked into the straw by hand to a depth of approximately 10 mm to create an optimal bond between the straw and the plaster. The second layer filled the formwork to the approximate plaster thickness. The third layer was a thin coat, applied by trowel, to ensure a smooth surface. A single batch of plaster was required per plaster skin. During the fabrication of the skin, three standard 50 mm cubes (per ASTM C109) and three standard 76 by 152 mm cylinders (per ASTM C39) were cast from the batch. The skin was allowed to set, then was covered by moist burlap. After six to

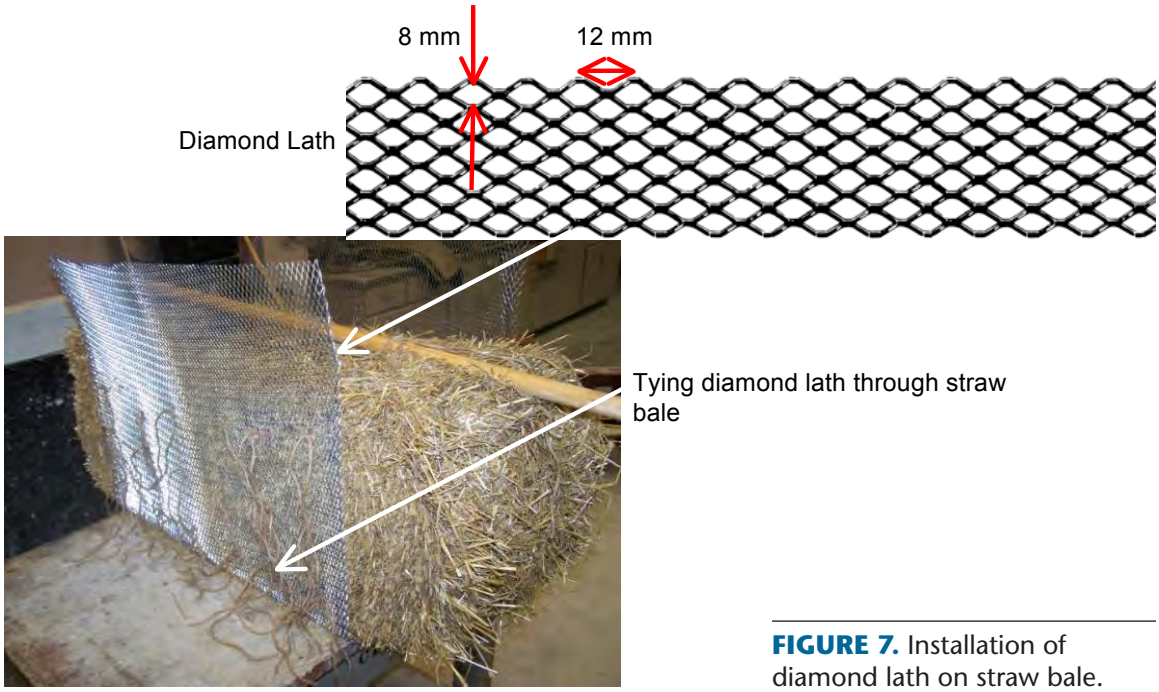

FIGURE 7. Installation of diamond lath on straw bale.

12 hours, the jig was rotated 180 degrees and the plastering process was repeated for the opposite face.

Upon setting of the plaster, the cubes and cylinders were removed from their forms and placed with the specimen under moist burlap and wrapped in plastic. The burlap was kept moist and the cubes, cylinders, and the plastered straw-bale assembly were cured under these conditions for three days.

Each plastered straw-bale assembly was subjected to three-point bending (Figure 8). Table 1 outlines the test program and the parameters examined. The height of each specimen was 330 mm. The span between the supports was varied between 200 mm and 500 mm to result in depth-to-span ratios (H/L) of 0.66 to 1.65. This range of values is typical of "deep beams", in which a significant amount of load is carried to supports by a compression strut between the load and reaction support (MacGregor and Bartlett 1999). The intention was to have specimens that would fail in flexure at wider spans, and due to plaster crushing (as arching action becomes dominant) at narrower spans.

FIGURE 8. Schematic of test set-up illustrating the test dimensions.

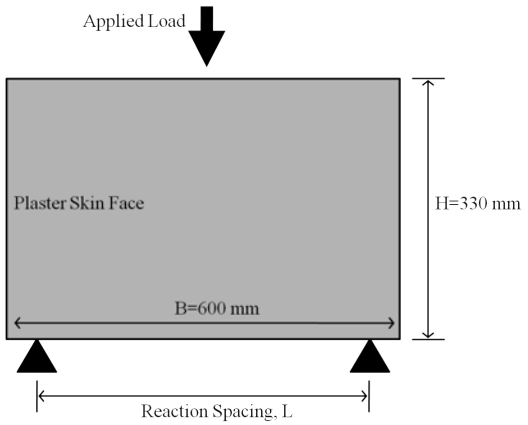

TABLE 1. Experimental parameters.

Specimen	Reaction Spacing, L (mm)	Reinforcement
1,2,3	500	None
4,5,6	400	None
7	300	None
8	250	None
9	200	None
10,11,12	400	Metal diamond lath

Within four to six weeks after fabrication, each specimen was placed in a universal testing machine, instrumented, and tested. Figure 9 shows the details of the test set-up. The load was applied from the test machine through a steel spreader beam (Figure 9a). The spreader beam plays a role similar to the top beam in a wall (Figure 1), transferring the load into the plastered bale assembly, leading to bending about the axis parallel to the spreader beam, similar to bending that occurs in a discontinuous region in a wall. Gauging plaster between the loading head and the spreader beam was used to ensure alignment of the test set-up. Fifty millimeter wide square steel pads with rollers were placed at each of the six contact points (Figure 9b and 9c). One was placed on top of each skin at the midpoint of the specimen (Figure 9b) and two were

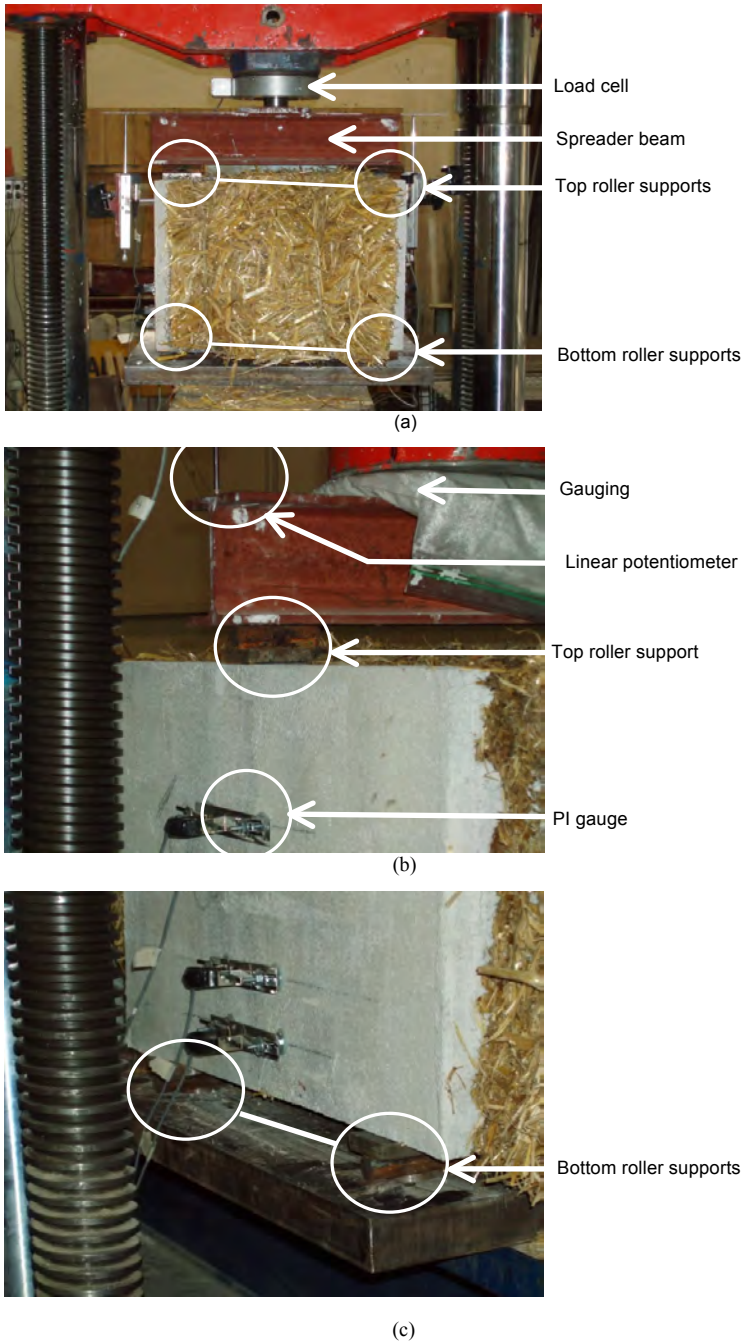

FIGURE 9. Specimen in universal testing machine: (a) Side view showing spreader beam; (b) Close-up showing typical top roller; (c) Close-up showing typical bottom roller.

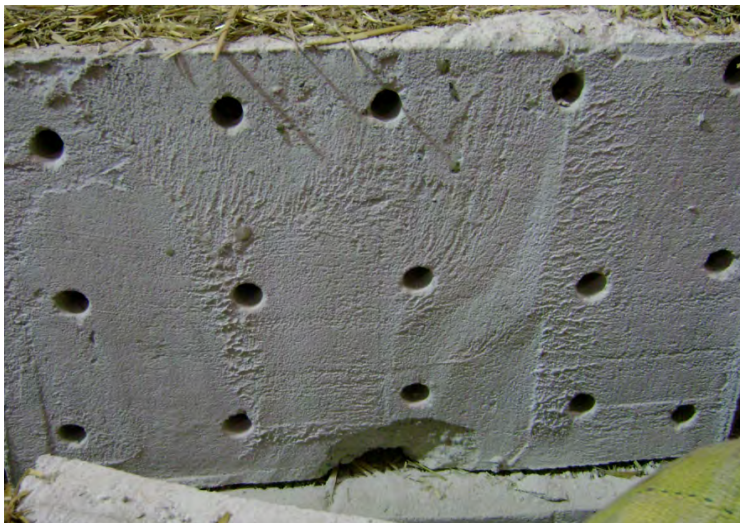

FIGURE 10. Holes drilled in the plaster skin after the completion of each test to permit measurements of the plaster thickness.

placed on the bottom surface of each skin (Figure 9c) spaced at distances of 200 to 500 mm center-to-center, depending on the spacing requirement of that test.

Each straw-bale assembly was instrumented with two linear potentiometers (LPs), and six 100 mm Pi Gauges (Figures 9b and 9c). The LPs were placed at positions enabling measurement of vertical deflections of each skin at the point of applied load (the top bearing pads) and were used, in part, to gauge the uniformity of load distribution to the skins. Three Pi Gauges were installed on each skin to measure horizontal strains along the vertical centerline. They were installed 50 mm, 100 mm, and 200 mm from the bottom. In later tests, a higher resolution of horizontal strain data was desired and the Pi Gauges were shifted towards the skin's lower edge at a distance of 20 mm, 50 mm, and 100 mm from the bottom.

The panels were tested in stroke-control at a rate of 0.1 mm/min. The test proceeded until a few minutes after the ultimate load was reached to record the pre- and post-failure behaviors. Upon completion of each test, 15 holes were drilled in each of the two plaster skins of the straw-bale and the depths were recorded to approximate the skin thickness at various locations. The plaster cubes and cylinders were tested following the procedures in ASTM C109 and C39, respectively.

Additional tests were carried out to quantify the tensile strength of the plaster. Six batches of the plaster were prepared. For each batch, 3 cube compression tests, and 3 split cylinder tests as per ASTM C496 were carried out.

RESULTS

Two distinct failure modes were observed during the testing. Specimens with an H/L value less than 1 (tests with span lengths of 400 mm and 500 mm) underwent tension failure of the plaster due to flexure (referred to as "flexural cracking" in the remainder of the paper). Specimens with H/L values greater than 1 failed by crushing of the plaster under the loading pads.

A typical load-deflection curve for a specimen with H/L < 1 is shown in Figure 11 (Specimen 6). The 'Top Deflection' values on the x-axis represent the vertical deflection of the top bearing pads. The curve's general shape was typical and represents all the characteristics of the

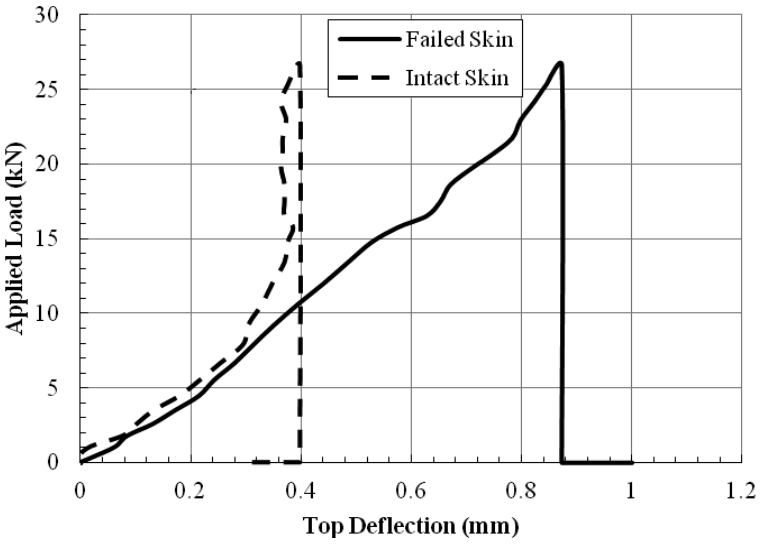

FIGURE 11. Load-deflection curve for Specimen 6.

curves found for the five other unreinforced specimens subjected to three-point bending with 400 and 500 mm reaction spacing.

Each of the six specimens with H/L < 1 failed when one plaster skin experienced failure by cracking (referred to as the "failed skin") while the other (referred to as the "intact skin") remained intact, showing no signs of failure. A large crack initiated at the bottom edge of the plaster skin halfway between the two reaction points and was approximately 5 mm in width. The crack immediately propagated upwards vertically, penetrating the top edge of the plaster skin and leaving only the straw to resist the load. The integrity of the bearing points remained, and no crushing of the plaster beneath the bearing pads was observed. Figure 12 shows a failure of this type.

The dotted line in Figure 11 represents the load vs. vertical deflection curve of the intact skin while the solid line shows that of the failed skin. Initially, the deflection in both skins was similar. This indicates that the top beam was loading each skin equally. At about 15% of the ultimate load, the curves for each skin began to diverge. The deflection of the intact skin increased at a much slower rate than the failed skin (note that at this point, neither skin has

FIGURE 12. Plastered straw bale panel, failed by vertical tensile cracking.

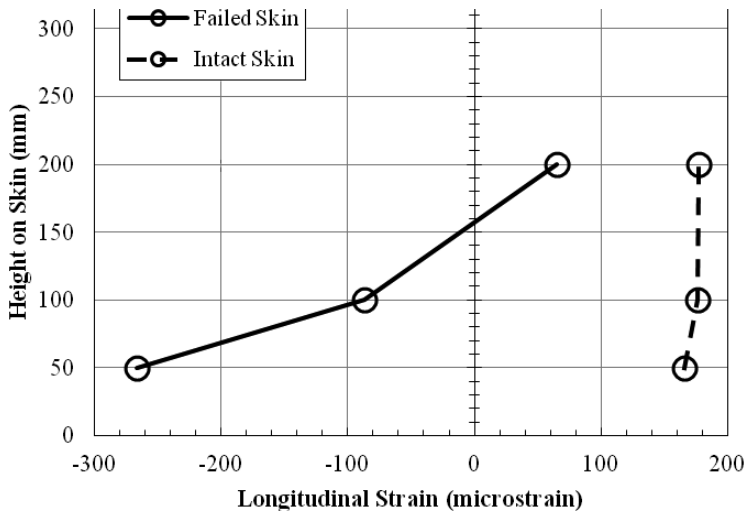

FIGURE 13. Strain distribution of plaster skins at the ultimate load of Specimen 6.

failed). This indicates that the top beam was rotating. At failure, there was about a 0.5 mm difference in the vertical deflection of the intact and failed skins. This is equivalent to a top beam rotation of 0.05 degrees. This divergence in deflections could be related to the difference in strength and stiffness of the plaster composing each skin. As loading increased, the weaker skin would begin to develop microcracks, leading to a reduction in stiffness and increased deflections on that side.

The strain distributions of the two plaster skins at the ultimate load of the panel are shown in Figure 13. Negative values of strain are in tension. At a height of 50 mm from the bottom of the failed skin, a longitudinal strain of –267 microstrain was recorded at the ultimate load. The extreme tensile strain was consistent with the observation of a tensile crack forming at failure. The tensile strain decreased with height and was approximately linear. The size of the tensile zone was approximately 150 mm from the bottom, or 46% of the plaster skin height. The strains measured on the intact skin were all compressive. Tensile strains may have occurred at a level lower than that at which Pi gauges were mounted. Nevertheless, the Pi gauge data indicates that the two plaster skins were not bending equally.

As the H/L ratio increased, the failure mode was observed to change from vertical tensile cracking at mid-panel to bearing failure at the loading point. The load-deflection curve for Specimen 8 is shown in Figure 14. The curve's general trend of the response is typical for unreinforced bales with span lengths of 200 mm, 250 mm, and 300 mm. At the ultimate load, one plaster skin experienced failure by crushing of the plaster beneath the top pad, while the other skin remained intact.

Up to 15% of the ultimate load, the load-deflection response of each plaster skin was identical. At this point, the curves began to diverge. Unlike the bales with 400 and 500mm span lengths, the failure was not accompanied by a total loss of load capacity. After the ultimate load was reached, the top bearing pad continued to crush the plaster beneath it. At this point, the residual strength of the straw-bale assembly was 40 to 60% of the ultimate strength.

The strain distribution at the ultimate load for Specimen 8 (Figure 15) indicates that the tensile strains that were developed in the failed skin were less than those measured for the tests with H/L > 1 (Figure 13). Note the Pi gauges were shifted towards the bottom

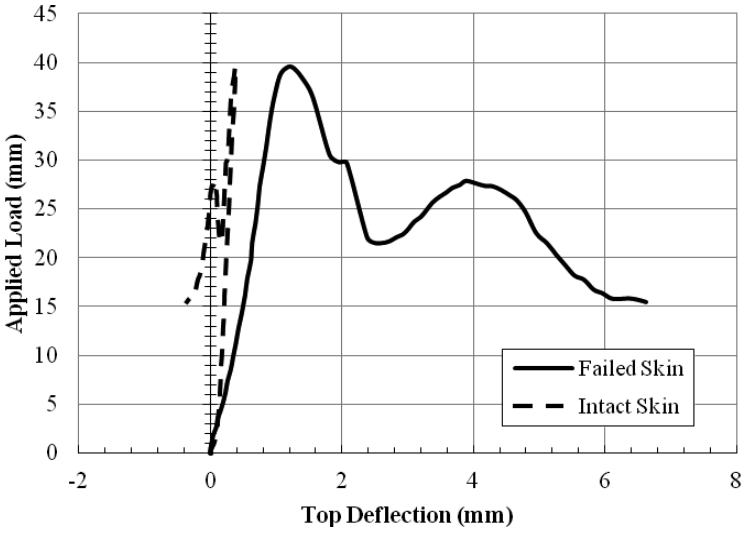

FIGURE 14. Load-deflection curve for Specimen 8.

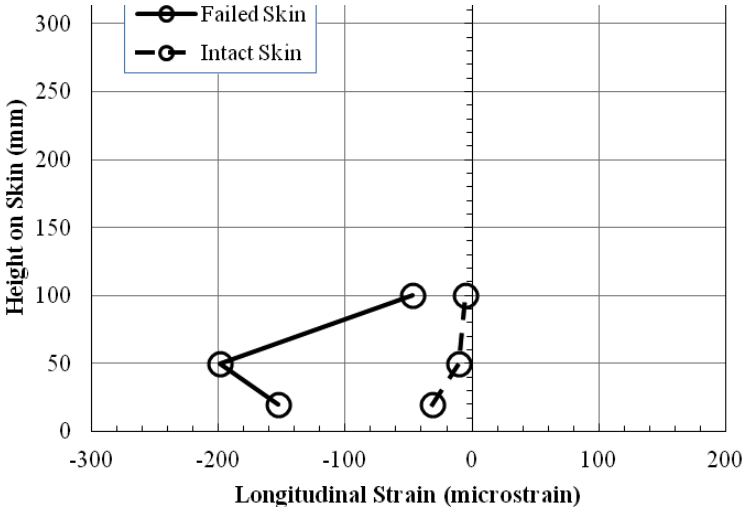

FIGURE 15. Strain distribution of plaster skins at the ultimate load of Specimen 8.

edge of the plaster skin for these tests. The strain measured by the Pi gauge located 20 mm from the bottom (–150 με) is less than that measured by the gauge 50 mm from the bottom (–200 με), which is not expected. However, the difference is within the precision of the Pi gauges (± 100 με). The strains in the intact skin were significantly less than those in the failed skin at the ultimate load, again indicated that the two skins were not being loaded evenly. The strain distribution, if extrapolated for both skins, suggests that the neutral axis is located between a height of 100 mm to 150 mm.

Figure 16 shows a typical failure for specimens subjected to three-point bending with support spacing between 200 and 300 mm. At the ultimate load, one skin crushed while the other remained intact. Crushing of the plaster in contact with the top bearing pad occurred while the plaster in contact with the two bottom bearing pads remained intact. No vertical tensile cracking was observed.

FIGURE 16. Plastered straw bale panel failed by plaster crushing at point of load application. Note that the holes in the plaster skin were drilled after the test was completed, and were used to measure the plaster thickness.

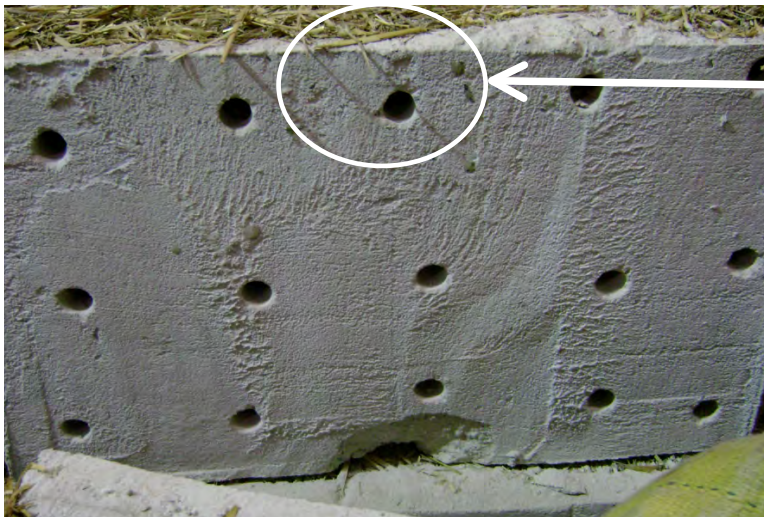

The reinforced specimens (Specimens 10, 11, and 12) were tested with a 400 mm span, and failed in the same manner as the unreinforced panels with 400 and 500mm support spacing; that is, at the ultimate load, a vertical tensile crack developed in one of the plaster skins while the other remained intact. The load-deflection curve for Specimen 11 is shown in Figure 17. Like the unreinforced bales, the behaviour of the two skins was similar up to 15% of the ultimate load. At that point, the deflections in the failed skin increased faster than the intact skin. At the ultimate load, sudden vertical cracking of the bottom plaster edge at mid-panel led to a rapid loss of strength. The crack immediately propagated upwards, penetrating to the top edge of the plaster skin. Unlike the unreinforced specimens of 400 and 500mm spacing, residual strength was present after the maximum load. The integrity of the bearing points remained and no crushing of the plaster beneath the bearing pads was observed. No rupture of the steel reinforcement was observed at failure. Instead, the plaster and diamond lath became debonded and the geometry of diamond shaped openings became skewed slightly.

The strains measured at failure for Specimen 11 are shown in Figure 18. As observed in the other tests, the tensile strains in the failed skin were higher than those in the intact skin. Extrapolating the data, the location of the neutral axis can be estimated as 30% and 60% of the height of the panel and the ultimate tensile strain in the plaster can be estimated to be between 250 and 300 microstrain.

Following the completion of each test, compression tests of cube samples of the plaster for each skin were completed. In addition, for most specimens, holes were drilled in each plaster skin and the plaster thickness measured in 15 locations on each skin. However, Specimens 4, 5, and 6 were inadvertently destroyed before plaster thicknesses could be measured. For these, the plaster thickness is estimated to be the nominal 25 mm. The results are summarized in Table 2. The 'Plaster Strength' is the average compressive strength of three cube specimen

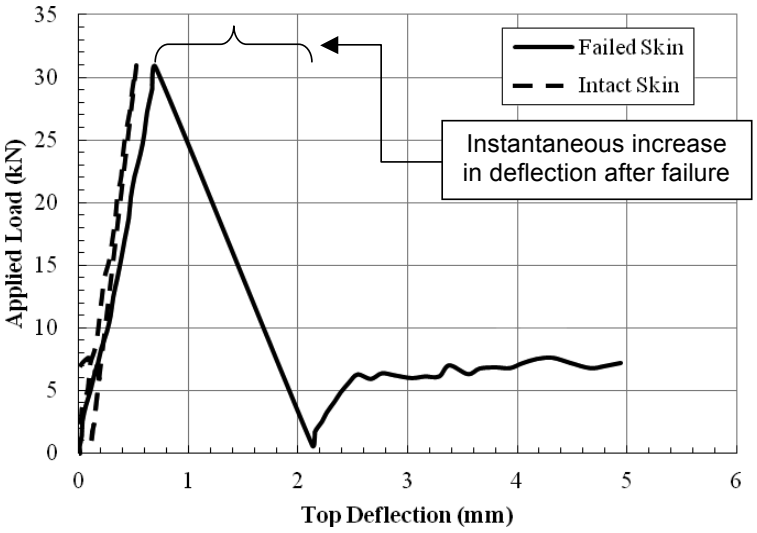

FIGURE 17. Load-deflection curve, Specimen 11.

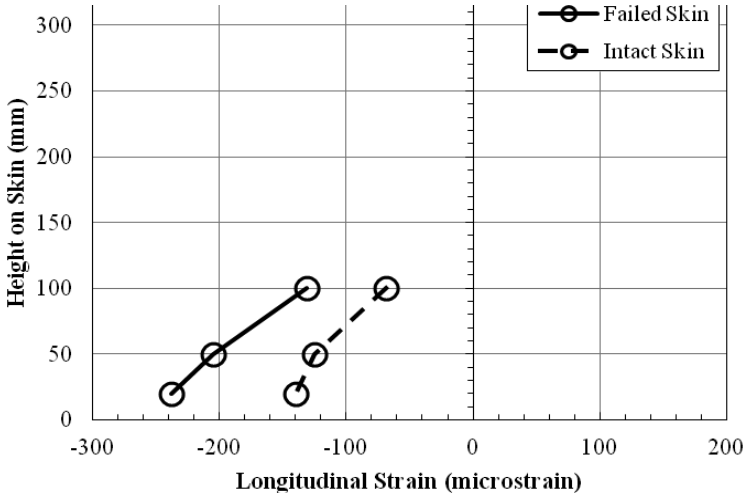

FIGURE 18. Strain distribution of plaster skins at the ultimate load of Specimen 11.

tests. The 'Average Skin Thickness' was the average depth of 15 holes drilled after experimentation. Also included in brackets is the standard deviation of the thickness measurements. The scatter in the plaster thickness is large, with the standard deviation ranging between 10% to 20% of the average value. The observed failure modes indicated that the bottom edge of the plaster skin (for flexural failure), and the top edge of the plaster skin (for bearing failure) were also critical. The 'Bottom Edge Skin Thickness at Mid-Panel' was the skin thickness at the bottom edge of the skin along the vertical centreline of the panel. The 'Top Bearing Edge Skin Thickness' was the thickness of the plaster in immediate contact with the top bearing pad.

The failure (or "peak") load for each test is summarized in Table 3, along with the observed failure modes. The term "Cracking" indicates failure by development of a tensile flexural crack in the plaster. The term "Crushing" indicates failure by compressive failure of the plaster in the vicinity of the top bearing plates.

TABLE 2. Summary of plaster skin results.

Test	Skin	Average Plaster Strength, f'_c [Standard deviation][1] (MPa)	Average Skin Thickness, t_{avg} [Standard deviation][2] (mm)	Bottom Edge Skin Thickness at Mid-Panel (mm)	Top Bearing Edge Skin Thickness (mm)
1	Failed	15.8 [1.2]	25 [4]	23	20
	Intact	13.6 [0.3]	35 [7]	35	43
2	Failed	15.3 [0.3]	31 [4]	28	36
	Intact	13.0 [0.2]	34 [4]	27	31
3	Failed	14.3 [1.3]	36 [7]	29	36
	Intact	13.0 [1.6]	37 [7]	46	40
4	Failed	13.6 [0.3]	25*	25*	25*
	Intact	19.6 [0.7]	25*	25*	25*
5	Failed	14.6 [0.6]	25*	25*	25*
	Intact	16.5 [0.3]	25*	25*	25*
6	Failed	20.5 [0.7]	25*	25*	25*
	Intact	17.0 [0.4]	25*	25*	25*
7	Failed	17.4 [2.8]	22 [4]	26	15
	Intact	16.8 [0.4]	33 [4]	41	27
8	Failed	14.6 [0.8]	35 [4]	33	28
	Intact	17.7 [1.6]	29 [4]	29	24
9	Failed	16.4 [0.3]	27 [4]	27	27
	Intact	16.3 [0.4]	39 [5]	40	34
10	Failed	17.0 [0.1]	31 [5]	30	23
	Intact	16.2 [0.5]	33 [3]	35	35
11	Failed	16.7 [1.0]	31 [4]	27	32
	Intact	16.6 [0.5]	33 [4]	27	36
12	Failed	17.0 [2.5]	31 [2]	30	32
	Intact	19.2 [0.9]	31 [3]	37	32

*thickness measurements were not taken. Nominal plaster thickness is used.
[1] Average and standard deviation calculated from 3 cube tests.
[2] Average and standard deviation calculated from 15 plaster thickness measurements.

DISCUSSION

The observed failure loads (Table 3) generally follow the expected trend. The average of the failure loads for the specimens tested at the 500 mm span (Specimens 1, 2, and 3) is 17.6 kN The average of the failure loads for the unreinforced specimens tested at the 400 mm span (Specimens 4, 5, and 6) is 27.3 kN. As would be expected, the failure load decreases as the span increases. For Specimens 7, 8, and 9, the failure loads were 19.47 kN, 39.69 kN, and

TABLE 3. Summary of failure loads.

Test	Skin	Ultimate Load [Failure Mode] (kN)	Predicted		P_{ult} predicted (kN)	Exp./Pred.
			Beam Model, Cracking Failure (kN)	Bearing Model, Crushing Failure (kN)		
1	Failed	17.55 [Crushing]	15	32	15	1.15
	Intact		20	58		
2	Failed	18.42 [Cracking]	18	55	18	1.00
	Intact		19	40		
3	Failed	16.93 [Cracking]	21	52	21	0.82
	Intact		21	52		
4	Failed	25.38 [Cracking]	18	34	18	0.95
	Intact		21	49		
5	Failed	29.58 [Cracking]	18	37	18	0.92
	Intact		20	41		
6	Failed	26.97 [Cracking]	22	51	20	0.85
	Intact		20	43		
7	Failed	19.47 [Crushing]	24	26	24	0.83
	Intact		35	45		
8	Failed	39.69 [Crushing]	41	41	37	1.06
	Intact		37	43		
9	Failed	43.38 [Crushing]	42	44	42	1.04
	Intact		60	55		
10	Failed	30.02 [Cracking]	32	39	32	0.93
	Intact		33	57		
11	Failed	31.23 [Cracking]	32	54	32	0.98
	Intact		34	60		
12	Failed	44.85 [Cracking]	32	54	32	1.40
	Intact		34	62		

43.38 kN, respectively. All were observed to fail by crushing below the top bearing pad, and so were expected to have failure loads higher than for Specimens 1–6, which all failed by development of a tensile flexural crack in the plaster. This is true except for Specimen 7, which has a failure load about 29% below the average failure load for Specimens 4, 5, and 6. This could indicate that Specimen 7 is an outlier, however, confounding the comparison are the differences in plaster strength and thickness, despite being nominally identical for all specimens.

A comparison can also be made between the reinforced bales tested at a span of 400 mm, Specimens 10, 11, and 12, which have an average strength of 35.4 kN, and the unreinforced

bales tested at the same span. The reinforced bales have a strength 30% higher on average than the unreinforced bales. Again, however, differences in plaster thickness and strength mean direct comparisons should be treated with caution.

To better deal with differences between the plaster characteristics for each specimen, two simple models are examined. The first assumes failure occurs at the location of maximum bearing stress, and is due to crushing in compression of the plaster:

$$P_{ult} = A_b f_c' \tag{1}$$

where A_b is the bearing area, and f_c' is the compressive strength.

The second model treats the plastered straw-bale as a beam in bending. The transformed section concept has been used to analyse straw-bale walls subjected to out-of-plane bending (King 2006). The straw is transformed to an equivalent area of plaster by multiplying the width of the bale by the modular ratio, n_{bale}:

$$n_{bale} = \frac{E_{bale}}{E_p} \tag{2}$$

where E_{bale} is the elastic modulus of the bale and E_p is the elastic modulus of the plaster. For the reinforced bales, the steel mesh reinforcement was transformed to an equivalent area of plaster by multiplying the area of the mesh by the modular ratio, n_s:

$$n_s = \frac{E_s}{E_p} \tag{3}$$

Assuming the bale acts as a Bernoulli beam in bending, the maximum moment at failure, M_{ult}, will be:

$$M_{ult} = S_t \sigma_{ult} \tag{4}$$

where S_t is the elastic section modulus based on the transformed section, and σ_{ult} is the material strength. The tensile strength of plaster is significantly smaller than the compressive strength, and so is likely to govern the strength of a plastered straw-bale in bending. Relationships between the cylinder compressive strength, f_c', and the tensile strength, f_t, of concrete are well known in the literature, for example (MacGregor and Bartlett 1999):

$$f_t = 0.53\sqrt{f_c'} \tag{5}$$

Note that the compressive strength in Equation 5 is for cylinder strength tests, while cube compression tests are typically used for plasters. Cube compression strength values are known to be on average about 20% higher than cylinder strength values (Vardy 2009). The applicability of Equation 5 to the low strength plasters used in straw-bale construction was investigated by comparing the cube compression strength to the tensile strength obtained from split cylinder tests for the plaster used for the tests carried out in this paper. Figure 20 shows the comparison. Each data point represents the average of 3 test values (i.e three cube compression tests and 3 split cylinder tests). The range of plaster strengths is small, as only one plaster design was tested. Nevertheless, the results suggest that Equation 5 can be used to estimate f_t for plasters falling within the range of strength values investigated in this paper.

The following assumptions and input data were used to predict the ultimate strength of the 12 specimens tested using Equations (1) and (4).

The plaster strength, f_c', used in Equation (1) was the measured cube strength given in Table 2 for each plaster skin. The bearing area was based on the width of the bearing pads (50 mm) and the measured top bearing skin thickness for the 2 skins, as given in Table 2.

The ultimate strength in Equation (4) was calculated using Equation (5) and the measured f_c' for each plaster skin. The modular ratios required values of the elastic modulus for each material. For the plaster, this can be determined using f_c' (Vardy 2009):

$$E_p = 818 f_c'$$

For straw, an average value of E_{bale} = 0.5 MPa was assumed based on Vardy (2009). Note that the modulus of the straw is so low compared to the plaster, that its transformed area is negligible compared to that of the plaster and straw. A nominal value of E_s = 200000 MPa was assumed for the steel mesh. The transformed section modulus, S_t, was calculated using the average plaster skin thickness (Table 2), and the average straw-bale width of 400 mm. The reinforcing mesh had openings of width 8 mm. Thus, over the 400 mm bale width, on average 50 mesh strands would be expected. Each strand had a nominal cross-sectional area of 2 mm^2. Therefore, a total steel cross-sectional area of 100 mm^2 was assumed. The interaction between the mesh and plaster is ignored.

In predicting the strength of the bale using Equation 4, it is assumed that the "spreader beam" (Figure 9a) carries exactly one-half the load to each plaster skin. The load-deflection plots and strain gauge data indicated that as the plastered straw-bale approached failure, the loading beam underwent rotations, and the "Failed" skin was more heavily loaded than the "Intact" skin. Nevertheless, uniform loading will be assumed in the calculations. Furthermore, this assumption means the ultimate load that corresponds to M_{ult} in Equation 4 can be determined from statics (i.e $P_{ult} = 4M_{ult} / L$). In considering the reinforced bales, it is assumed that the steel mesh has not undergone yielding at the ultimate load. This is based on the measured strains at the ultimate from the testing. The maximum tensile strains ranged between 250 με to 300 με. Given an elastic modulus of steel of 200000 MPa, this is equivalent to a stress in the steel of between 50 MPa to 60 MPa.

Table 3 summarizes the predicted ultimate strengths and compares them to the experimental values. Average plaster strengths and thickness values were measured for both skins of each bale, and predictions were made for each potential failure mode, and for each plaster skin. The lowest of the predicted strength values was taken as the predicted P_{ult}. These values are compared to the experimental values in the final column of the table. In general, the comparison between the predicted and experimental values is acceptable. The average experimental to predicted ratio for all 12 tests is 0.96, with a range of 0.82 to 1.40. The upper range is high because of Specimen 12, which may represent an outlier. In any event, the equations predicted a conservative strength for the bale. An average difference between the predicted and experimental values of 4% is small considering the scatter in the plaster strength, and the crude method required to measure the plaster thickness.

The results indicate that simple principles of mechanics can be used to analyse a plastered straw-bale assembly subjected to 3 point bending. In particular, it is possible to use Equations 1 and 4 to predict the ultimate strength for a range of H/L values such that the failure mode transitions from a bearing type (shear dominated) failure to a flexural failure. For H/L < 1, flexural failure governed by tensile fracture of the plaster dominates. The presence of steel mesh reinforcement does not change this failure mode, however, the mesh does increase the

strength. For H/L > 1, failure is dominated by crushing of the plaster in compression. Flexural cracking of the plaster in tension does not occur.

The results suggest that current practice for straw bale construction is generally appropriate. To avoid tensile cracking of plaster due to flexure, regions around doors, windows, and other openings should be designed such that H/L > 1. This is typically the case around doorways. Around window openings, this is often not the case, however, the results of this study indicate that the use of steel reinforcing mesh can increase the plastered bale strength by 30% on average in these regions.

CONCLUSIONS

Twelve plastered straw-bale panels of equal height but of varied span lengths and reinforcement type were tested under three-point bending. The panels failed by either crushing of the plaster skin at the bearing-plaster interface or by vertical cracking propagating from the bottom edge at mid-panel. For assemblies subjected to 3-point bending and H/L > 1, failure is governed by the compressive strength of the plaster. For assemblies subjected to 3-point bending and H/L < 1, failure is dominated by flexure and governed by the tensile strength of the plaster.

The results have shown that the ultimate strength of the panels can be accurately predicted based on the strength of the plaster, the dimensions of the specimen, and the geometry of loading, using simple principles of mechanics. A transformed section approach can be used to predict the strength of plastered straw-bales, either unreinforced, or reinforced with steel mesh.

The results suggest that current practice for straw bale construction is generally appropriate. To avoid tensile cracking of plaster due to flexure, regions around doors, windows, and other openings should be designed such that H/L > 1. In regions where H/L < 1, the use of steel reinforcing mesh can increase the plastered bale strength by 30% on average.

REFERENCES

Ashour, T., Bahnasawey, A., Wu, W. (2010) *Compressive strength of fibre reinforced earth plasters for straw bale buildings.* Australian Journal of Agricultural Engineering, Vol. 1, No. 3, pp. 86–92.

ASTM C39 (2004) *Standard Test Method for Compressive Strength of Cylindrical Concrete Specimens*, American Society for Testing of Materials, West Conshohocken, Pennsylvania.

ASTM C109 (1998) *Standard Test Method for Compressive Strength of Hydraulic Cement Mortars (Using 2-in. or [50-mm] Cube Specimens*, American Society for Testing of Materials, West Conshohocken, Pennsylvania.

ASTM C150 (2007) *Standard Specification for Portland Cement*, American Society for Testing of Materials, West Conshohocken, Pennsylvania.

ASTM C207 (2006) *Standard Specification for Hydrated Lime for Masonry Purposes*, American Society for Testing of Materials, West Conshohocken, Pennsylvania.

ASTM. C496 (2004) *Standard Test Method for Splitting Tensile Strength of Cylindrical Concrete Specimens*. American Society for Testing of Materials. West Conshohocken, Pennsylvania, USA.

Gross, C., Fovargue, J., Homer, P., Mander, T., Walker, P., and White, C. (2009) *Lateral Stability of Prefabricated Straw Bale Housing*. Sustainability in Energy and Buildings, Part 3, pp. 147–154.

Kim, Y.J, Reberg, A., and Hossain, M. (2011) *A Conceptual Development of Reinforced Plastered Straw Bale Composite Sandwich Walls.* Journal of Performance of Constructed Facilities, post on-line ahead of print January 20, 2011.

King, B. (2006). *Design of Straw Bale Buildings: The State of the Art*. Green Building Press.

MacGregor, J., and Bartlett, F. (1999). *Reinforced Concrete: Mechanism and Design (Canadian Ed.)*. Pearson Education Canada.

Parker, A. Aschheim, M., Mar, D., Hammer, M., and King, B. (2006) *Recommended mesh anchorage details for straw bale walls.* Journal of Green Building, Vol. 1, No. 4, pp. 3–13.

Vardy, S., and MacDougall, C. (2006) *Compressive Testing and Analysis of Plastered Straw Bales*, Journal of Green Building, Vol. 1, No. 1, pp. 65–79.

Vardy, S., and MacDougall, C. (2007) *Compressive Response of Plastered Straw Bale Wall Panels*, International Conference on Sustainable Construction Materials and Technologies, Coventry, UK, June 2007, pp. 789–800.

Vardy (2009) *Structural Behaviour of Plastered Straw Bale Assemblies Under Concentric and Eccentric Loading*, PhD Thesis, Queen's University, Kingston, Ontario, Canada: 329 pages.